



# ChemSusChem

Chemistry–Sustainability–Energy–Materials

 **Chemistry  
Europe**

European Chemical  
Societies Publishing

## Accepted Article

**Title:** Immobilization of a molecular Re complex on MOF-derived hierarchical porous carbon for CO<sub>2</sub> electroreduction in water/ionic liquid electrolyte

**Authors:** Marc Fontecave, Domenico Grammatico, Huan Ngoc Tran, Yun Li, Silvia Pugliese, Laurent Billon, and Bao-Lian Su

This manuscript has been accepted after peer review and appears as an Accepted Article online prior to editing, proofing, and formal publication of the final Version of Record (VoR). This work is currently citable by using the Digital Object Identifier (DOI) given below. The VoR will be published online in Early View as soon as possible and may be different to this Accepted Article as a result of editing. Readers should obtain the VoR from the journal website shown below when it is published to ensure accuracy of information. The authors are responsible for the content of this Accepted Article.

**To be cited as:** *ChemSusChem* 10.1002/cssc.202002014

**Link to VoR:** <https://doi.org/10.1002/cssc.202002014>

WILEY-VCH

1 **Immobilization of a molecular Re complex on**  
2 **MOF-derived hierarchical porous carbon for**  
3 **CO<sub>2</sub> electroreduction in water/ionic liquid**  
4 **electrolyte**

7 *Domenico Grammatico,<sup>a,c</sup> Dr. Huan Ngoc Tran,<sup>b</sup> Dr. Yun Li,<sup>b</sup> Silvia Pugliese,<sup>a,b</sup>*

8 *Prof. Laurent Billon,<sup>c</sup> Prof. Bao-Lian Su<sup>a,\*</sup> and Prof. Marc Fontecave<sup>b,\*</sup>*

9  
10 <sup>a</sup> Laboratory of Inorganic Materials Chemistry (CMI), University of Namur, 61 rue de  
11 Bruxelles, B-5000 Namur, Belgium.

12  
13  
14 <sup>b</sup> Laboratoire de Chimie des Processus Biologiques, UMR CNRS 8229, Collège de France-  
15 CNRS-Sorbonne Université, PSL Research University, 11 Place Marcelin Berthelot, 75005  
16 Paris, France.

17  
18 <sup>c</sup> Bio-inspired Materials Group: Functionality & Self-assembly, Université de Pau et des Pays  
19 de l'Adour, E2S UPPA, CNRS, IPREM UMR 5254, 64000, PAU, France

20  
21 \* to whom correspondence should be addressed : [marc.fontecave@college-de-france.fr](mailto:marc.fontecave@college-de-france.fr);  
22 [bao-lian.su@unamur.be](mailto:bao-lian.su@unamur.be)

23  
24 **KEYWORDS:** CO<sub>2</sub> electroreduction; catalysis; rhenium complex; heterogenization;  
25 hierarchical porous carbon; ionic liquid

27 **Abstract**

28 The development of molecular catalysts for CO<sub>2</sub> electroreduction within electrolyzers requests  
29 their immobilization on the electrodes. While a variety of methods have been explored for the  
30 heterogenization of homogeneous complexes, we here report a novel approach using a  
31 hierarchical porous carbon material, derived from a Metal Organic Framework, as a support for  
32 the well-known molecular catalyst [Re(bpy)(CO)<sub>3</sub>Cl] (bpy = 2,2'-bipyridine). This cathodic  
33 hybrid material, named Re@HPC, has been tested for CO<sub>2</sub> electroreduction using a mixture of  
34 an ionic liquid (1-Ethyl-3-methylimidazolium tetrafluoroborate, EMIM) and water as the  
35 electrolyte. Interestingly, it catalyzes the conversion of CO<sub>2</sub> into a mixture of carbon monoxide  
36 and formic acid, with a selectivity that depends on the applied potential. The present study thus  
37 reveals that Re@HPC is a remarkable catalyst, enjoying excellent activity (turnover numbers  
38 for CO<sub>2</sub> reduction of 7835 after 2 h at -1.95 V vs Fc/Fc<sup>+</sup> with a current density of 6 mA cm<sup>-2</sup>)  
39 and good stability. These results emphasize the advantages of integrating molecular catalysts  
40 onto such porous carbon materials for developing novel, stable and efficient, catalysts for CO<sub>2</sub>  
41 reduction.

## 42 Introduction

43 Carbon dioxide electroreduction into energy-dense carbon-based liquid or gaseous products is  
44 an attractive way to store renewable energies into chemical energy. However, because of the  
45 high stability of CO<sub>2</sub> and the requirement of multiple electron- and proton-transfers for its  
46 transformation, catalysts are required to overcome the slow kinetics, minimize activation  
47 energies and overpotentials and control product selectivity. While heterogeneous catalysts are  
48 generally favored due to their stability as well as facile product and catalyst recovery,  
49 homogeneous molecular metal complexes (coordination and organometallic complexes) have  
50 also been developed for CO<sub>2</sub> electroreduction since the 1980's. In particular, they offer the  
51 unique opportunity to tune the coordination environment of the metal center and its reactivity  
52 *via* synthetic modifications of the ligands. The molecular strategy has been recently described  
53 in review articles.<sup>[1,2]</sup>

54 To reconcile these two approaches, homogeneous catalysts have sometimes been immobilized  
55 on heterogeneous conductive supports in order to provide original hybrid electrodes. However,  
56 this strategy has been applied to few molecular catalysts with limited success so far in the  
57 specific case of CO<sub>2</sub> electroreduction.<sup>[3-5]</sup> To illustrate the various techniques developed for  
58 providing access to such hybrid electrodes, the case of the prototypical catalyst  
59 [Re(bpy)(CO)<sub>3</sub>Cl] (bpy = 2,2'-bipyridine), highly selective for CO<sub>2</sub> to CO conversion, is  
60 interesting, since its immobilization has been studied using a variety of approaches. The first  
61 attempts to immobilize this complex were achieved by Meyer and coworkers<sup>[6]</sup> and Abruña  
62 and coworkers<sup>[7]</sup> in 1985 and 1986 respectively, two years after the initial publication by Lehn  
63 reporting the catalytic activity of this complex for CO<sub>2</sub> reduction.<sup>[8]</sup> In both cases, the catalyst  
64 was immobilized *via* electropolymerization of [Re(vbpy)(CO)<sub>3</sub>Cl] (vbpy = 4-vinyl-4'-methyl-  
65 2,2'-bipyridine) on an electrode to afford catalytic poly-[Re(vpby)(CO)Cl] films, allowing  
66 electroreduction of CO<sub>2</sub> to CO with very high faradaic yields in CH<sub>3</sub>CN. However, these films  
67 were shown to exhibit limited stability. A similar polymerization approach was recently  
68 developed by Kubiak and co-workers using 5-ethynyl-bipyridine derivatives, instead of vinyl-  
69 bipyridine, however in that case very fast deactivation of the catalytic films was observed.<sup>[9]</sup> A  
70 different strategy for electropolymerization of a variant of [Re(bpy)(CO)<sub>3</sub>Cl] was reported by  
71 Deronzier and co-workers.<sup>[10]</sup> Upon electrochemical oxidation of a solution of  
72 [Re(pyrbpy)(CO)<sub>3</sub>Cl] (pyrbpy = 4-(4-Pyrrol-1-ylbutyl)4'-methyl-2,2'-bipyridine) using a Pt  
73 electrode, a polypyrrole-based film was deposited and found to catalyze the electroreduction of  
74 CO<sub>2</sub> in CH<sub>3</sub>CN leading to CO as the only reduction product. However, the polymer was highly

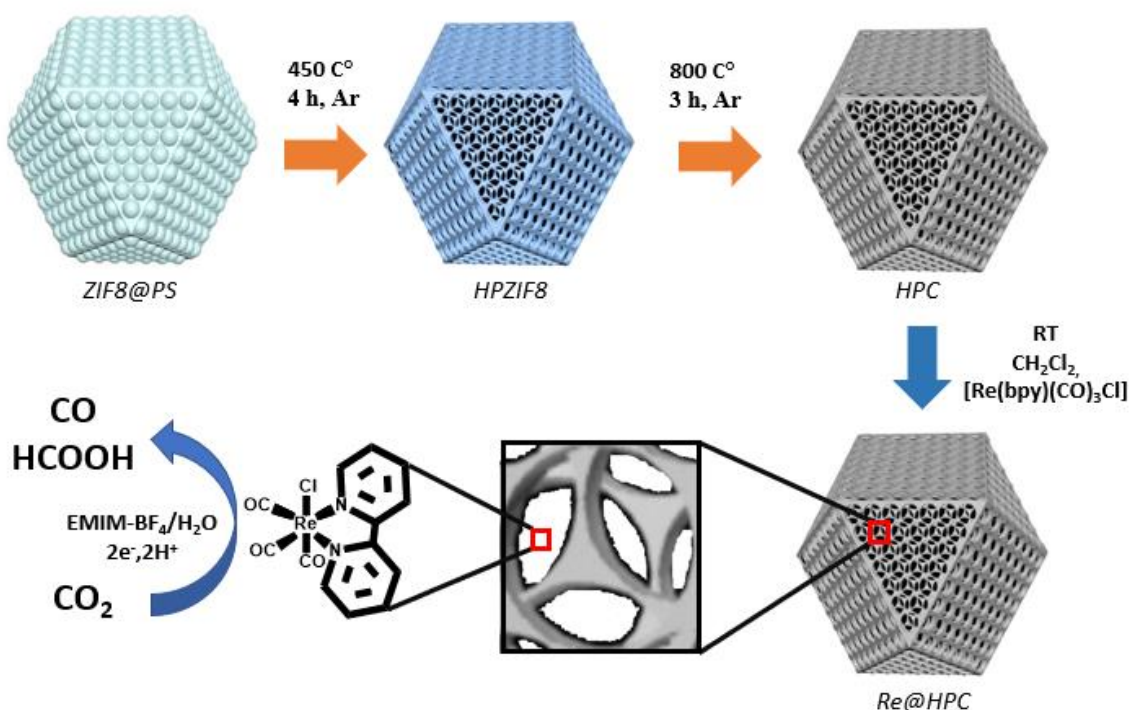
75 unstable and substantial loss of current was observed during electrolysis. In 1993, Kaneko and  
76 co-workers reported the immobilization, *via* simple adsorption, of [Re(bpy)(CO)<sub>3</sub>Br] within a  
77 Nafion<sup>®</sup> membrane, which is stable in various solvents and easily interfaces with electrode  
78 surfaces.<sup>[11]</sup> The polymer-confined catalyst was active for CO<sub>2</sub> electroreduction in neutral  
79 aqueous electrolyte, leading to mixtures of CO, H<sub>2</sub> and formic acid, with a selectivity depending  
80 on the applied potential.

81 Besides this immobilization strategy involving polymers and membranes, covalent grafting to  
82 the electrode has also been explored. As *o*-quinone moieties found on the edge planes of  
83 graphite can condense with substituted *o*-phenylenediamines, [Re(5,6-diamino-  
84 phenanthroline)(CO)<sub>3</sub>Cl] was used to modify graphite electrodes.<sup>[12]</sup> The increased conjugation  
85 between the catalyst and the electrode was proposed to overcome poor conductivity issues in  
86 some polymeric films deposited onto electrodes. This system was very selective for CO  
87 formation (faradaic yield of 96%) in CH<sub>3</sub>CN with high turnover numbers (TONs). A conjugated  
88 polymer material incorporating [Re(bpy)(CO)<sub>3</sub>Cl] motifs and covalently attached to a glassy  
89 carbon electrode was obtained by electropolymerization of a Re complex containing 2,2'-  
90 bipyridine-5,5'-bis-(diazonium) ligands.<sup>[13]</sup> These polymer films proved highly stable, allowing  
91 thousands of turnovers for selective production of CO in CH<sub>3</sub>CN. As a last illustration of this  
92 class of grafting methods, a [Re(4-(4-aminophenetyl)-4'-methyl-2,2'-bipyridine)(CO)<sub>3</sub>Cl]  
93 complex has been attached to a high surface area porous carbon electrode via the  
94 electrooxidation of the amino group.<sup>[14]</sup> While efficient for selective CO<sub>2</sub> to CO conversion,  
95 very fast leaching of the complex into the bulk solution was observed after few minutes of  
96 electrolysis.

97 Finally, non-covalent immobilization was achieved, exploiting  $\pi$ - $\pi$  interactions between  
98 pyrolytic graphite and [Re(pyrene-bpy)(CO)<sub>3</sub>Cl], containing a pyrene-substituted bpy.<sup>[15]</sup> This  
99 system was catalytically active for CO production but was rapidly deactivated, likely because  
100 of reduction of the pyrenyl moiety. The best result with such a non-covalent immobilization  
101 strategy was obtained by Kubiak and co-workers who developed a hybrid electrode resulting  
102 from the incorporation of [Re(tBu-bpy)(CO)<sub>3</sub>Cl], with tBu-bpy = 4,4'-di-*tert*-butyl-2,2'-  
103 bipyridine, into multi-walled carbon nanotubes (MWCNTs). This material proved stable and  
104 active in an aqueous electrolyte for highly selective CO production, at relatively low  
105 overpotential and with a current density of 4 mA cm<sup>-2</sup>.<sup>[16]</sup>

106 One of the drawbacks of all these immobilization strategies, with the exception of the MWCNT/  
107 [Re(tBu-bpy)(CO)<sub>3</sub>Cl] system, resides in the need to introduce functionalities to the bipyridine

108 ligand. This not only generates synthetic issues but also results in significant modifications of  
 109 the electronic properties of the catalyst as well as of its reactivity. We thus thought of  
 110 developing methods that allow the immobilization of the  $[\text{Re}(\text{bpy})(\text{CO})_3\text{Cl}]$  itself without  
 111 synthetic modifications. Here we report the preparation and characterization of an original  
 112 conductive carbon porous material and its utilization as a support for the  $[\text{Re}(\text{bpy})(\text{CO})_3\text{Cl}]$   
 113 catalyst, which can be easily fixed within the pores of the solid material. The novel hybrid  
 114 material proved stable and active as a catalyst for  $\text{CO}_2$  electroreduction, with high current  
 115 densities and high turnover numbers. Interestingly, this catalyst converts  $\text{CO}_2$  into a mixture of  
 116  $\text{CO}$  and  $\text{HCOOH}$ , whose ratio depends on the applied potential.  
 117



118

119

120 **Scheme 1:** Synthesis of HPC and Re@HPC.

121

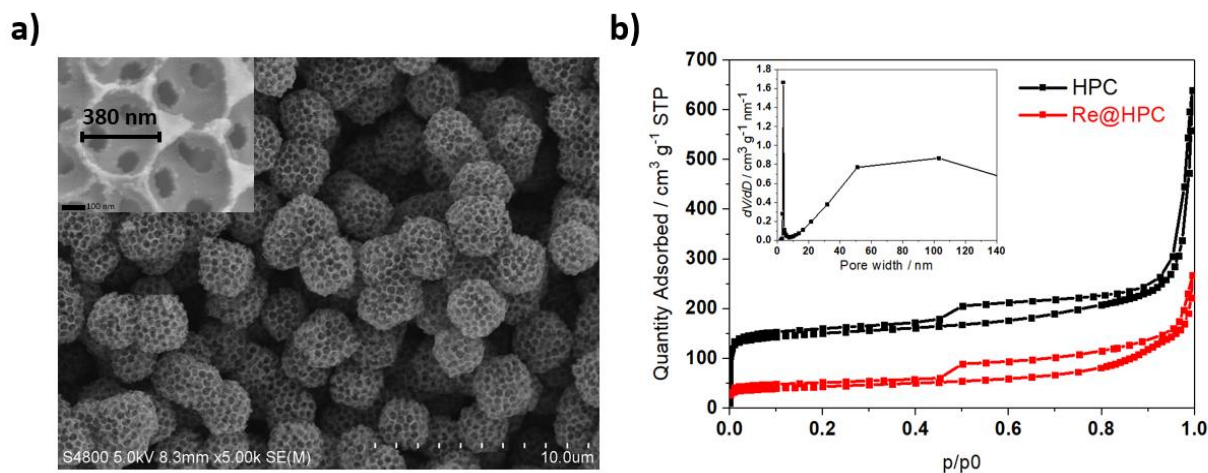
## 122 RESULTS AND DISCUSSION

### 123 Synthesis and characterization of the hierarchical porous ZIF8-derived carbon-HPC

124 The synthesis of hierarchical porous carbon (named HPC in the following) derived from the  
 125 Metal Organic Framework ZIF8 was synthesized following a previous report,<sup>[17]</sup> however with  
 126 significant modifications (Scheme 1). Briefly, the ZIF8 precursor was first infiltrated into the

127 polystyrene spheres (PS) template and crystallized using a solution of  $\text{CH}_3\text{OH}/\text{NH}_3\cdot\text{H}_2\text{O}$ .  
128 Second, a treatment at  $450\text{ }^\circ\text{C}$  under argon atmosphere, instead of washing with organic  
129 solvents used in the previous report,<sup>[17]</sup> was carried out in order to remove the PS template and  
130 thus obtain the hierarchical porous ZIF8 (HPZIF8). HPZIF8 shows slightly lower BET surface  
131 area (Figure S1 and Table S1) as compared to the previous report,<sup>[17]</sup> likely due to remaining  
132 PS beads in the sample. Scanning electronic microscope (SEM) and powder x-ray diffraction  
133 (XRD) characterizations of HPZIF8 show expected well-defined ZIF8 crystals (Figures S2-S3).  
134 HPZIF8 was finally pyrolyzed under an inert atmosphere at  $800\text{ }^\circ\text{C}$  to obtain the final  
135 hierarchical porous carbon (HPC) material. HPC was characterized by various techniques. XRD  
136 pattern confirmed that the material was not crystalline anymore (Figure S2). SEM images  
137 (Figure 1a and Figure S3c) showed well-defined and well-distributed carbon particles with a  
138 three-dimensional tetrakaidecahedron morphology and with a uniform monodisperse diameter  
139 of  $2\text{ }\mu\text{m}$ . This specific morphology is due to the use of PS as a template which controls the  
140 shape of the material.<sup>[17]</sup> The highly ordered porous carbon material showed a hexagonal close-  
141 packed arrangement of pores (inset Figure 1a) with interconnected windows and porosity  
142 uniformly distributed.<sup>[18,19]</sup>  $\text{N}_2$  physisorption analyses (Figure 1b and Figure S1) allowed to  
143 establish a BET surface area of  $495\text{ m}^2\text{ g}^{-1}$  and total pore volume of  $1\text{ cm}^3\text{ g}^{-1}$  with around 25%  
144 of the total pore volume assigned, by the Horwart-Kawazoe method, to the micropores. The  
145 increase of the surface area due to the pyrolysis step leading to HPC ( $495\text{ m}^2\text{ g}^{-1}$ ) from HPZIF8  
146 ( $145\text{ m}^2\text{ g}^{-1}$ ) is likely due to a complete removal of PS.  $\text{N}_2$  adsorption isotherms are of typical  
147 type I, indicating the microporous character of the material with a pore size of  $0.5\text{ nm}$ . The  
148 presence of mesopores and macropores has been revealed by two  $\text{N}_2$  adsorption uptakes at  $p/p_0$   
149 of  $0.5$  and  $0.95-1.0$ , respectively, as shown in Figure 1b. The BJH analysis method gave a very  
150 sharp peak centered at  $5\text{ nm}$ , corresponding to the hysteresis loop at  $p/p_0$  of  $0.5$ ,<sup>[20]</sup> while the  
151 sharp  $\text{N}_2$  adsorption uptake at  $p/p_0$  of  $0.95-1.0$  is generated by the macropores with a diameter  
152 of  $380\text{ nm}$  observed by SEM (Figure 1a). The above analysis suggests HPC material contains  
153 a hierarchical macro-meso-microporous structure.

154



155

156 **Figure 1:** a) SEM image of HPC with enlargement (inset); b) N<sub>2</sub> adsorption-desorption  
 157 isotherms of HPC and Re@HPC and pore size distribution for HPC (inset) made by BJH  
 158 method.

159

### 160 Functionalization of HPC material with a molecular complex

161 HPC was then used as a support for heterogenizing the molecular [Re(bpy)(CO)<sub>3</sub>Cl] complex,  
 162 named Re in the following. Re was immobilized without any further functionalization taking  
 163 advantage of the interconnected porosity of the support which improves the hosting properties.  
 164 The heterogenization of Re on HPC has been carried out as follows. Briefly, Re was first  
 165 dissolved in CH<sub>2</sub>Cl<sub>2</sub> and the solution added dropwise to a sonicated dispersion of HPC in the  
 166 same solvent, with an initial Re:HPC weight ratio of 1:9 (Scheme 1). After stirring the solution  
 167 for 1 h and centrifugation the as-obtained solid hybrid system, named Re@HPC, was dried  
 168 overnight at room temperature. Then, Re@HPC was characterized not only to check for the  
 169 presence of the molecular complex within the solid but also to define morphology and structure  
 170 of the final material.

171 SEM images of Re@HPC showed that the morphology of the carbon particles was retained  
 172 (Figure S4). The presence of Re within the solid has been verified by Energy Dispersive X-Ray  
 173 mapping (EDX) (Figure S4) showing a uniform dispersion of the complex, as well as the  
 174 presence of residual Zn from ZIF8, even after pyrolysis. N<sub>2</sub> physisorption analysis after Re  
 175 loading showed a decrease of the BET surface area in agreement with the incorporation of the  
 176 molecular complex within the pores of the support (Figure 1b). The integrity of Re within the  
 177 solid material was proved by <sup>1</sup>H NMR spectroscopy after releasing the complex from Re@HPC  
 178 by washing with CDCl<sub>3</sub>. The spectrum of the solution proved identical to that of the pure freshly  
 179 prepared homogeneous complex (Figure S5). Finally, the amount of extractable complex from



180 30 mg of Re@HPC using an organic solvent ( $\text{CH}_2\text{Cl}_2$ ) was determined by UV-Visible  
181 spectroscopy from the intensity of the absorption band at 387 nm, characteristic of the complex  
182 (Figure S6). We thus determined that the sample contained 4.8  $\mu\text{mol}$  of complex leading to 0.16  
183  $\mu\text{mol mg}^{-1}$  of complex within Re@HPC.

184

### 185 **Preparation and characterization of the working Re@HPC/GDL electrode**

186 An Re@HPC/GDL electrode ( $1 \text{ cm}^2$ ) was prepared by deposition of 5 mg Re@HPC on a  
187 commercial gas diffusion layer (GDL), as described in the experimental section. The total  
188 amount of Re in that electrode was determined after extraction by UV-Visible spectroscopy as  
189 described above for Re@HPC (Figure S6). The electrode was shown to contain 0.6  $\mu\text{mol cm}^{-2}$ .  
190 The CV of Re@HPC/GDL electrode in 0.1 M TBAPF<sub>6</sub> in  $\text{CH}_3\text{CN}$  at low scan rate of  $10 \text{ mV s}^{-1}$   
191 (Figure S7) served to calculate the density of electroactive species from the charge integration  
192 of the peak at about -1.6 V vs Fc/Fc<sup>+</sup>, corresponding to the reoxidation of the complex.<sup>[21]</sup> The  
193 data led to a surface density of 20  $\text{nmol cm}^{-2}$ , corresponding to approximately 3% of the total  
194 amount of complex present in the solid material. These numbers compare well with those  
195 determined for the best hybrid [Re(tBu-bpy)(CO)<sub>3</sub>Cl]/MWCNT material (13  $\text{nmol cm}^{-2}$ , 1-8%  
196 of the total catalyst loaded) reported by Kubiak *et al.*<sup>[16]</sup> Finally, the electrochemical active  
197 surface area of the electrode was determined as 2.18  $\text{cm}^2$  per 1  $\text{cm}^2$  of geometric surface area  
198 by a standard method (Figure S8).

199

### 200 **Electrocatalytic CO<sub>2</sub>RR in water/1-Ethyl-3-methylimidazolium tetrafluoroborate** 201 **(EMIM) electrolyte**

202 Since the electroreduction of CO<sub>2</sub> using the Re@HPC/GDL in water yielded mainly hydrogen  
203 (data not shown), the reaction was studied in a CO<sub>2</sub>-saturated solution of an ionic liquid in the  
204 presence of a small amount of water as a source of protons. Indeed, ionic liquids have been  
205 shown to facilitate CO<sub>2</sub> electroreduction catalyzed by solid catalysts due to their ability to  
206 increase CO<sub>2</sub> solubility and activate CO<sub>2</sub>.<sup>[22]</sup> A previous report showed that using an ionic liquid  
207 as both the solvent and electrolyte resulted in decreased overpotential and increased second-  
208 order rate constant for CO<sub>2</sub> electroreduction to CO catalyzed by [Re(bpy)(CO)<sub>3</sub>Cl].<sup>[23]</sup>  
209 However, with such homogeneous systems, the viscosity of the medium results in strong  
210 limitations in mass transport (small diffusion coefficients) of the molecular catalyst and low  
211 current densities. This issue does not apply to an immobilized molecular complex. Thus, a  
212 mixture of an ionic liquid (1-Ethyl-3-methylimidazolium tetrafluoroborate) and water (named

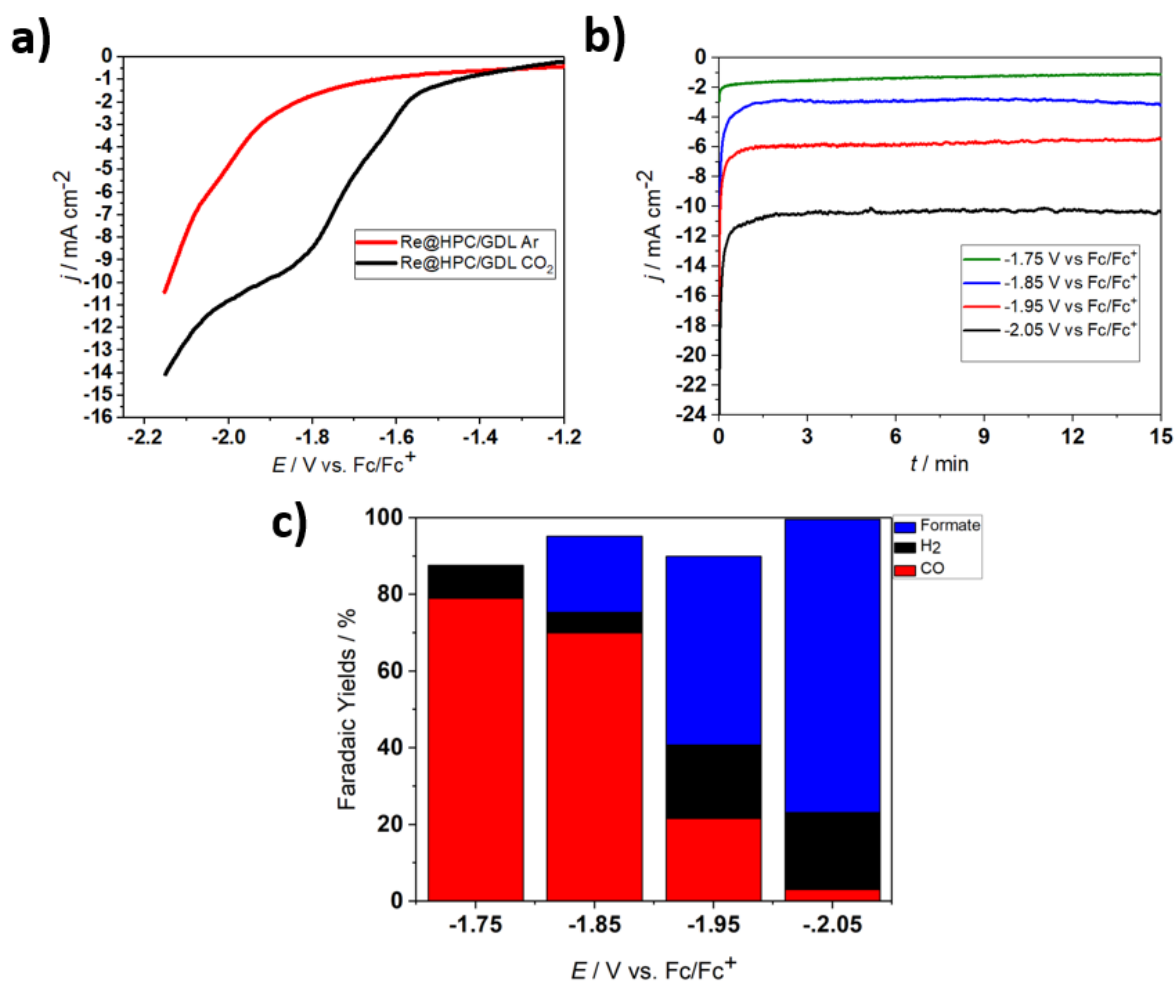
213 H<sub>2</sub>O/EMIM in the following) has been chosen as the electrolyte for further CO<sub>2</sub>  
214 electroreduction studies using the Re@HPC/GDL electrode. The Linear Sweep  
215 Voltammograms (LSVs) of the Re@HPC/GDL electrode in 5% v/v H<sub>2</sub>O/EMIM saturated with  
216 either Ar or CO<sub>2</sub> are presented in Figure 2a. A catalytic wave at an onset potential of -1.55 V  
217 vs Fc/Fc<sup>+</sup> and developing further up to an applied potential of -2.05 V was observed only in the  
218 presence of CO<sub>2</sub> and was thus assigned to CO<sub>2</sub> reduction (Figure 2a). At potentials more  
219 negative than -2.1 V, a second wave was observed however also present for the Re@HPC/GDL  
220 electrode under argon, thus likely corresponding to proton reduction to H<sub>2</sub>. Unfortunately, the  
221 evaluation of overpotential values is not trivial here as the equilibrium potentials of the  
222 CO<sub>2</sub>/HCOOH and CO<sub>2</sub>/CO couples in H<sub>2</sub>O/EMIM are unknown.

223 Controlled Potential Electrolysis (CPE) at different potentials between -1.75 V and -2.05 V vs  
224 Fc/Fc<sup>+</sup> coupled with quantification of CO<sub>2</sub> reduction products has been carried out for 15 min  
225 in order to characterize the CO<sub>2</sub> reduction reaction. As expected the total current density  
226 increased with increased driving force up to 11 mA cm<sup>-2</sup> at -2.05 V and was found to be stable  
227 during electrolysis at all potentials (Figure 2b). The high current densities translate into  
228 remarkably high turnover numbers (TONs) and high Turnover Frequencies (TOFs). For  
229 example, at -2.05 V, 2026 TONs were reached after 15 min, which corresponds to a TOF value  
230 of 2.3 s<sup>-1</sup>. As shown below, under these conditions, formate was the major product.

231 The only detected products in all experiments were H<sub>2</sub> and CO in the gaseous phase and formic  
232 acid in the liquid phase. Surprisingly, the selectivity of the reaction was found to be greatly  
233 dependent on the applied potential, with CO being the major product at the most anodic  
234 potentials and formic acid becoming the major product at potentials more cathodic than -1.9 V,  
235 while H<sub>2</sub> was a minor product at all potentials. This is clearly shown in Figure 2c which displays  
236 the Faradaic yields (FY) of the various products at different potentials. At -1.75 V vs Fc/Fc<sup>+</sup>,  
237 FY(CO) and FY(H<sub>2</sub>) were 79% (TON<sub>CO</sub> 260 and TOF<sub>CO</sub> 0.3 s<sup>-1</sup>) and 9% respectively, and no  
238 formate could be found in the liquid phase. Screening the reaction at more negative potentials,  
239 CO formation decreased dramatically while FY(HCOOH) and FY(H<sub>2</sub>), the latter to a smaller  
240 extent, increased. At -2.05 V, FY(CO), FY(H<sub>2</sub>) and FY(HCOOH) were 3%, 20% and 76%  
241 (TON<sub>HCOOH</sub> 1950 and TOF<sub>HCOOH</sub> 2.2 s<sup>-1</sup>) respectively (Figure 2c). Thus, the selectivity between  
242 CO vs HCOOH formation during electroreduction of CO<sub>2</sub> catalyzed by Re@HPC can be finely  
243 tuned by varying the applied potential.

244 As expected, the selectivity could also be tuned with the water content. When the 15 min CPE  
245 was carried out at -1.75 V vs Fc/Fc<sup>+</sup> in 10% v/v H<sub>2</sub>O/EMIM, the current was slightly larger but

246 the system was less selective for CO<sub>2</sub> reduction with a FY(H<sub>2</sub>) of 33 % (Figure S9). When  
 247 instead the water content was decreased (1% v/v H<sub>2</sub>O/EMIM), lower current densities were  
 248 obtained, with comparable selectivity. The 5% v/v H<sub>2</sub>O/EMIM electrolyte thus proved a good  
 249 compromise for achieving high current densities and high selectivity for CO<sub>2</sub> reduction (Figure  
 250 S9).  
 251



252  
 253 **Figure 2:** Controlled potential electrolysis of CO<sub>2</sub> using the Re@HPC/GDL electrode: **a)** LSV  
 254 in 5% v/v H<sub>2</sub>O/EMIM saturated with CO<sub>2</sub> (black) or with Ar (red), scan rate 20 mV s<sup>-1</sup>; **b)** total  
 255 current density at various applied potentials as a function of time; **c)** Faradaic Yields for CO,  
 256 H<sub>2</sub> and formate after 15 min electrolysis at different potentials in 5% v/v H<sub>2</sub>O/EMIM saturated  
 257 with CO<sub>2</sub>.  
 258

259 Production of formate is unexpected since the Re complex is known to be a very selective  
 260 catalyst for CO<sub>2</sub> electroreduction to CO in organic solvents. Interestingly, when, as a control  
 261 experiment, CPE was carried out using the soluble Re complex in the same CO<sub>2</sub>-saturated 5%  
 262 v/v H<sub>2</sub>O/EMIM electrolyte, the reaction was shown to yield mainly H<sub>2</sub> with minor amounts of  
 263 CO and almost no HCOOH, at all visited potentials (Figure S10). Furthermore, the current

264 densities were much lower since at -1.85 V the current density reached a value of 0.3 mA cm<sup>-2</sup>  
265 (Figure S10) for 12 μmol of Re catalyst (1 mM in 12 ml) as compared to 3 mA cm<sup>-2</sup> for 0.6  
266 μmol Re catalyst present in Re@HPC/GDL (Figure 2). This thus demonstrates the great impact  
267 of the solid support on the reaction outcome, both in terms of the activity and the selectivity.  
268 The effect on the activity is likely to be partly due to the hydrophobic nature of the environment  
269 provided by the pores in which the catalyst is bound, favouring CO<sub>2</sub> uptake and increasing CO<sub>2</sub>  
270 local concentration and to the absence of mass transport limitations which challenge the  
271 homogeneous catalyst.

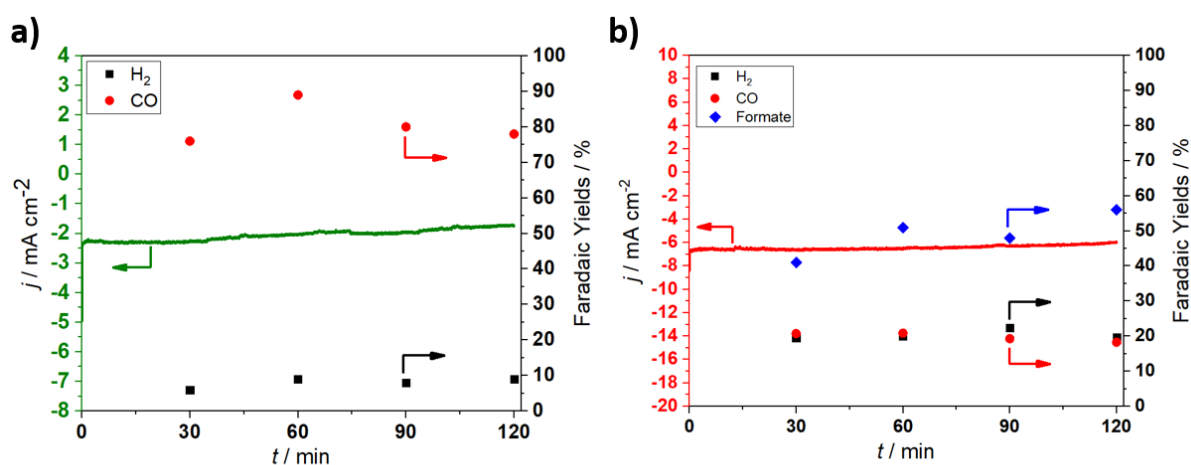
272 In contrast, the effect of the solid support on the selectivity is difficult to explain. Formation of  
273 formate cannot be explained by the catalytic properties of the support itself since, as a control  
274 experiment, CPE of CO<sub>2</sub> using an HPC/GDL electrode, not loaded with the Re complex, under  
275 identical conditions, gave very different results (Figure S11). For example, at -1.85 V, with a  
276 current density of 1 mA cm<sup>-2</sup>, no formate could be detected, as compared to 3 mA cm<sup>-2</sup> and a  
277 FY(HCOOH) of 20% for the Re@HPC/GDL electrode, and, at -1.95 V, with a current density  
278 of 2 mA cm<sup>-2</sup>, a FY(HCOOH) of 15% was obtained, as compared to 6 mA cm<sup>-2</sup> and a  
279 FY(HCOOH) of 50% for the Re@HPC/GDL electrode. These results confirm that the specific  
280 catalytic properties of the Re@HPC/GDL electrode are essentially due to the immobilized Re  
281 complex, with limited or no contribution from the residual Zn. Formation of formate also  
282 excludes Zn as an active species since this metal is well-established for selective formation of  
283 CO. [24]

284 There is, to our knowledge, one study reporting formate production during electroreduction of  
285 CO<sub>2</sub> catalyzed by the Re complex, with a HCOOH/CO selectivity depending on the applied  
286 potential as well. [11] Interestingly, in that case, the catalyst was incorporated into a Nafion  
287 membrane and electrolysis was carried out in a phosphate aqueous electrolyte, explaining why  
288 the major product at almost all potentials applied was H<sub>2</sub>. The activity, in terms of current  
289 density, of that system was furthermore much lower than that reported here. While formate  
290 production using the Re@HPC catalyst is likely to proceed *via* a Re-H hydride species reacting  
291 with CO<sub>2</sub>, [25,26] in contrast to CO production which derives from a Re-CO<sub>2</sub> intermediate, it is so  
292 far unclear why the HPC support favours such a mechanism at very cathodic potentials and how  
293 the support tunes the HCOOH/CO selectivity. These mechanistic aspects deserve further  
294 investigation.

295

296 Finally, CPE was carried out for 2 h at -1.75 V (FY(CO)=80% and FY(H<sub>2</sub>)=10%) and -1.95 V  
 297 (FY(CO)=20%, FY(H<sub>2</sub>)=20% and FY(HCOOH)=55%) vs Fc/Fc<sup>+</sup> (Figure 3). The system  
 298 proved very stable during electrolysis in terms of both current density and selectivity. After 2 h  
 299 at -1.75 V, 3155 TON<sub>CO</sub> were achieved corresponding to a TOF<sub>CO</sub> of 0.4 s<sup>-1</sup>. Furthermore, post-  
 300 electrolysis characterization of the electrode by SEM showed that the porosity of the system  
 301 was retained even if slight agglomeration of the particles was observed (Figure S12). After 2 h  
 302 at -1.95 V, 7835 TONs (TON<sub>CO</sub> + TON<sub>HCOOH</sub>) were achieved corresponding to a TOF (TOF<sub>CO</sub>  
 303 + TOF<sub>HCOOH</sub>) of 1.1 s<sup>-1</sup>. A longer experiment, during 5 hours, confirmed the stability of the  
 304 catalyst (Figure S13).

305



306

307 **Figure 3:** Two-hour electrolysis: current density and FY as a function of time during CPE at -  
 308 1.75 V vs Fc/Fc<sup>+</sup> (a) and at -1.95 V vs Fc/Fc<sup>+</sup> (b) under CO<sub>2</sub> in 5% v/v H<sub>2</sub>O/EMIM using the  
 309 Re@HPC/GDL electrode. Faradaic yields for CO (red dots), H<sub>2</sub> (black squares) and formate  
 310 (blue diamonds).

311

## 312 Conclusion

313

314 We have developed a novel hybrid solid catalyst, Re@HPC, for CO<sub>2</sub> electroreduction to CO  
 315 and HCOOH. Thanks to the hierarchical porosity of the porous and conductive carbon material  
 316 HPC, large amounts of the molecular catalyst [Re(bpy)(CO)<sub>3</sub>Cl] can be easily immobilized  
 317 without any functionalization. We anticipate that HPC can be further used for heterogeneization  
 318 of other complexes. In order to optimize catalysis, CO<sub>2</sub> electroreduction has been studied in an  
 319 ionic liquid electrolyte in the presence of water, known to favour CO<sub>2</sub> solubility and activation.  
 320 To the best of our knowledge, this is the first example of a heterogeneized molecular complex

321 characterized for CO<sub>2</sub> reduction catalysis in an ionic liquid. Re@HPC/GDL electrodes thus  
322 provide high current densities (up to 11 mA cm<sup>-2</sup>), high TOF<sub>CO+HCOOH</sub> (2.3 s<sup>-1</sup>) and display good  
323 stability. When compared to other hybrid solid electrodes in which [Re(bpy)(CO)<sub>3</sub>Cl] has been  
324 immobilized,<sup>[6-12,14-16]</sup> the Re@HPC/GDL electrode clearly shows significant improvements  
325 in terms of catalyst loading, TOF values and, most remarkably, in terms of stability: with the  
326 exception of the MWCNT/ [Re(tBu-bpy)(CO)<sub>3</sub>Cl] material developed by Kubiak and  
327 collaborators<sup>[16]</sup>, all previously Re-based hybrid catalysts greatly suffer from low stability  
328 (Table S3). It is also interesting to note that the Re@HPC/GDL electrode compares well, in  
329 terms of current density at comparable potentials, with a standard CO-selective Ag electrode in  
330 a CH<sub>3</sub>CN/EMIM electrolyte.<sup>[27]</sup> In addition, this novel electrode is unique in providing not only  
331 CO but also HCOOH as CO<sub>2</sub> reduction products, with FY(H<sub>2</sub>) not exceeding 20%, in marked  
332 contrast with the other comparable systems which are selective for CO production and in  
333 contrast with the homogeneous catalyst which favours proton reduction over CO<sub>2</sub> reduction and  
334 is quite inefficient in the same water/ionic liquid system. The CO/HCOOH ratio can be tuned  
335 with the applied potential since it decreased as the potential is shifted to more cathodic values.  
336 The combination of a water/ionic liquid electrolyte system, the hierarchical porosity of the  
337 support facilitating mass exchange and transfer,<sup>[28]</sup> and the hydrophobic environment provided  
338 by the pores in which the molecular complex is fixed is likely to explain the remarkable and  
339 unique performances of Re@HPC as a CO<sub>2</sub> reduction catalyst. However, further studies are  
340 required to understand how the support drives and controls the reactivity of the immobilized  
341 complex.

342

343

344

## 345 **Experimental section**

### 346 **General methods**

347 All chemicals were received from commercial sources and used as received. Zinc nitrate  
348 hexahydrate ( $\text{Zn}(\text{NO}_3)_2 \cdot 6\text{H}_2\text{O}$ , 99%), 2-methylimidazole (98%), tetrabutylammonium  
349 hexafluorophosphate (TBAPF<sub>6</sub>, 98%), Nafion<sup>®</sup> perfluorinated resin (10  $\mu\text{L}$  of a 5 wt% solution  
350 in mixture of lower aliphatic alcohols containing 5% water), absolute ethanol ( $\text{CH}_3\text{CH}_2\text{OH}$ ),  
351 methanol ( $\text{CH}_3\text{OH}$ , 99%), dichloromethane ( $\text{CH}_2\text{Cl}_2$ , 99 %), acetonitrile ( $\text{CH}_3\text{CN}$ , 99.8%),  
352 chloroform-d ( $\text{CDCl}_3$ , 99.8%) and ammonia solution ( $\text{NH}_3 \cdot \text{H}_2\text{O}$ , 32% ) were purchased from  
353 Sigma-Aldrich. 1-Ethyl-3-methylimidazolium tetrafluoroborate (>98%) was purchased from  
354 IOLITEC Ionic liquid technologies GmbH.  $[\text{Re}(\text{bpy})(\text{CO})_3\text{Cl}]$  was synthesized as previously  
355 reported by Kubiak *et al.*<sup>[29]</sup>

356 UV–vis spectra were recorded using a Cary 100 UV–vis spectrophotometer (Agilent). <sup>1</sup>H  
357 spectra were recorded on a Bruker Avance-III 300 NMR spectrometer (300 MHz) at room  
358 temperature. The Rhenium concentrations in the electrolyte were assessed using an Agilent  
359 7900 quadrupole ICP-MS. Liquid samples were sprayed through a micro-nebulizer in a Scott  
360 spray chamber prior to ionization. An indium internal standard was injected after inline mixing  
361 with the samples to correct for signal drift. Calibration solutions with Re concentrations  
362 encompassing the full range of sample concentrations were used to convert measured counts to  
363 concentrations. Reported uncertainties were calculated using algebraic propagation of blank  
364 subtraction and sample count standard deviations (n=3).

### 365 **Material characterization**

366 Scanning electron microscope (SEM) images were performed by using a JEOL 7500F  
367 microscope operating at 15kV with EDX detector incorporated and a Hitachi S-4800 operating  
368 at 5kV. X-ray diffraction (XRD) characterization was carried out by Panalytical X'Pert PRO  
369 diffractometer (Cu K $\alpha$  radiation, Bragg-Brentano geometry, sealed tube operated at 45 mA 30  
370 kV X'Celerator linear detector). Nitrogen physisorption analyses were performed with ASAP  
371 2420 using a platinum resistance device and liquid nitrogen as adsorbed molecule.

### 372 **Synthesis of HPZIF8**

373 Polystyrene spheres (PS) (the size of 400 nm) were synthesized as previously reported<sup>[17]</sup> and  
374 used as a template for the preparation of a hierarchical porous ZIF8 (HPZIF8). ZIF8 with  
375 polystyrene (ZIF8@PS) was also prepared using a protocol from Chen *et al.*<sup>[17]</sup>, via infiltration  
376 of the ZIF8 precursor into the PS spheres template. The following steps were modified from

377 the previous protocol to obtain the HPZIF8. This, was prepared from ZIF8@PS treating it at  
378 450 °C during 4 h under Argon atmosphere for removing the PS beads.

### 379 **Synthesis of HPC**

380 The hierarchical porous carbon (HPC) derived from ZIF8 was obtained by heating the HPZIF8  
381 at 800 °C during 3 h under Argon atmosphere. The HPC was used without further treatment.

### 382 **Preparation of Re@HPC**

383 The preparation of Re complex loading on HPC material was carried out as follows: the solution  
384 of [Re(bpy)(CO)<sub>3</sub>Cl] (6 mg) in CH<sub>2</sub>Cl<sub>2</sub> (10 mL) was added dropwise to a sonicated dispersion  
385 of HPC (50 mg) in CH<sub>2</sub>Cl<sub>2</sub> (20 mL). The suspension was then centrifuged for removing the  
386 supernatant. The obtained material was then dried overnight under vacuum condition at room  
387 temperature and used without further treatments.

388 These materials were characterized by: N<sub>2</sub> physisorption analyses, SEM images, EDX mapping  
389 and XRD (Supporting Information).

390 The amount of Re complex loaded was quantified by UV-Visible spectroscopy (Figure S6):  
391 after extraction of 30 mg of Re@HPC with 20 mL of CH<sub>2</sub>Cl<sub>2</sub> the solution was analysed for its  
392 absorption at 387 nm, characteristic of [Re(bpy)(CO)<sub>3</sub>Cl] and the latter was compared to  
393 calibration curve prepared with pure [Re(bpy)(CO)<sub>3</sub>Cl]. Re@HPC was also treated with CDCl<sub>3</sub>  
394 for extraction of the complex and characterization by <sup>1</sup>H NMR (Figure S5), in order to confirm  
395 the integrity of the complex.

### 396 **Electrode preparation**

397 Re@HPC (5 mg) was sonicated 1 h in absolute ethanol (200 μL) and a solution of Nafion  
398 perfluorinated resin (10 μL of a 5 wt% solution in mixture of lower aliphatic alcohols containing  
399 5% water). The suspension was then, carefully, deposited by drop casting on a gas-diffusion  
400 Layer, GDL (AVCarb GDS 3250; 1 cm<sup>2</sup>) in order to have a uniform deposition. The electrode  
401 was then dried in air overnight at room temperature. For all the experiments the working  
402 electrodes were prepared in the same way.

### 403 **Electrode characterization**

404 SEM images of the Re@HPC/GDL electrode were obtained before and after 2 h electrolysis.  
405 The amount of Re complex present on the GDL was quantified by UV-Visible spectroscopy as  
406 described above via extraction of the complex from the Re@HPC/GDL electrode immersed in  
407 20 mL of CH<sub>2</sub>Cl<sub>2</sub> (Figure S6) and quantification by comparison with the calibration curve.



## 408 **Electrochemical characterization**

409 All electrochemical characterization and electrolysis experiments were carried out using a Bio-  
410 logic SP300 potentiostat with two-compartment cell with an Ag/AgCl/3M KCl reference  
411 electrode, placed in the same compartment as the working Re@HPC/GDL electrode. A  
412 platinum counter electrode was placed in a separate compartment. The two compartments were  
413 separated by a membrane (Fumasep FBM-Bipolar Membrane). The electrolyte was CO<sub>2</sub>-  
414 saturated 5% v/v H<sub>2</sub>O/EMIM (12.5 mL). The electrochemical cell was first purged with CO<sub>2</sub> at  
415 a flow rate of 20 mL min<sup>-1</sup> for 1 h prior to catalytic tests using a mass flow controller (Bronkhorst  
416 EL-FLOW model F-201CV). All potential values are given versus the potential of the Fc/Fc<sup>+</sup>  
417 couple added as an internal standard to the solution after measurement. In 5% v/v H<sub>2</sub>O/EMIM:  
418 E<sub>1/2</sub>(Fc/Fc<sup>+</sup>) = 0.35V vs Ag/AgCl (Figure S14).

419 Electrochemically active surface area of the electrode was estimated by probing the redox  
420 reaction of the ferricyanide/ferrocyanide couple using cyclic voltammetry (CV). 0.1 M KCl  
421 solution containing 25 mM ferrocyanide was initially degassed with Ar. Then the potential of  
422 the working electrode was swept between 700 mV and -200 mV vs. Ag/AgCl (1 M KCl) at  
423 different scan rates (mV s<sup>-1</sup>). Between each CV at different rates, the solution was bubbled with  
424 Ar and shaken to quickly reach back to the initial conditions. Electrochemically active surface  
425 areas (ECSA) were estimated from the Randles-Sevcik equation, as follows:

$$426 \quad I_p = (2.69 \times 10^5) n^{3/2} A D^{1/2} \nu^{1/2} C$$

427 with I<sub>p</sub>: peak current, n: number of moles of electrons per mole of electroactive species, A: area  
428 of electrode (cm<sup>2</sup>), D: diffusion coefficient (cm<sup>2</sup> s<sup>-1</sup>), ν: scan rate (V s<sup>-1</sup>), C: concentration (mol  
429 cm<sup>-3</sup>). The diffusion coefficient of ferricyanide is 6.7 × 10<sup>-6</sup> cm<sup>2</sup> s<sup>-1</sup> and its concentration 25 ×  
430 10<sup>-6</sup> mol cm<sup>-3</sup>. The ECSA (A) is estimated from the slope of the plot of I<sub>p</sub> versus ν<sup>1/2</sup>.

431 CVs for the determination of surface density of electrochemically active sites were recorded in  
432 CH<sub>3</sub>CN, 0.1 M TBAPF<sub>6</sub> with a scan rate of 10 mV s<sup>-1</sup>.

433 The surface loading (Γ[Re] as mol cm<sup>-2</sup>) of the catalyst was calculated through the integration  
434 of the reoxidation wave in the CV scan (Figure S7) using the equation:

$$435 \quad \Gamma[\text{Re}] = \frac{q}{nFA}$$

436 where q is the charge (C) obtained from integration of the oxidation wave, n the number of  
437 electrons in the redox process per Re center (n = 1), F is the Faraday constant (96485 C mol<sup>-1</sup>),  
438 and A is the geometrical electrode area (1 cm<sup>2</sup>).<sup>[30]</sup>

439 The homogeneous electrochemical experiments were carried out under the same conditions  
440 described above using the same electrochemical cell. A glassy carbon electrode (1 cm<sup>2</sup>) was  
441 used as working electrode in a solution 1 mM of [Re(bpy)(CO)<sub>3</sub>Cl] in 5% v/v H<sub>2</sub>O/EMIM.  
442 H<sub>2</sub> and CO were identified and quantified using a gas chromatograph (SRI 8610C) equipped  
443 with a packed Molecular Sieve 5 Å column for permanent gases separation and a packed  
444 Haysep-D column for light hydrocarbons separation. Argon (Linde 5.0) was used as carrier gas.  
445 A flame ionization detector (FID) coupled to a methanizer was used to quantify CO while a  
446 thermal conductivity detector (TCD) was used to quantify H<sub>2</sub>. The liquid-phase products were  
447 quantified using an ionic exchange chromatography system (883 Basic IC plus; Metrohm).

448

449

#### 450 **Acknowledgements**

451 *D.G and S.P acknowledge financial support from the European School on Artificial Leaf:*  
452 *Electrodes & Devices (eSCALED). This work is part of the eSCALED project which has*  
453 *received funding from the European's Union's Horizon 2020 research and innovation*  
454 *programme under the Marie Skłodowska-Curie grant agreement No 765376.*

455 *This research used resources of the Electron Microscopy Service located at the University of*  
456 *Namur. This Service is member of the "Plateforme Technologique Morphologie –Imagerie".*

457 *SEM images were also collected by F. Pillier at the Laboratoire Interfaces et Systèmes*  
458 *Electrochimiques, Paris, France.*

459

460 **References**

- 461 [1] R. Francke, B. Schille, M. Roemelt, *Chem. Rev.* **2018**, *118*, 4631–4701.
- 462 [2] H. Takeda, C. Cometto, O. Ishitani, M. Robert, *ACS Catal.* **2017**, *7*, 70–88.
- 463 [3] N. Elgrishi, M. B. Chambers, X. Wang, M. Fontecave, *Chem. Soc. Rev.* **2017**, *46*, 761–
- 464 796.
- 465 [4] C. Sun, R. Gobetto, C. Nervi, *New J. Chem.* **2016**, *40*, 5656–5661.
- 466 [5] L. Sun, V. Reddu, A. C. Fisher, X. Wang, *Energy Environ. Sci.* **2020**, *13*, 374–403.
- 467 [6] T. R. O’Toole, L. D. Margerum, T. D. Westmoreland, W. J. Vining, R. W. Murray, T. J.
- 468 Meyer, *J. Chem. Soc. {,} Chem. Commun.* **1985**, 1416–1417.
- 469 [7] C. R. Cabrera, H. D. Abruña, *J. Electroanal. Chem. Interfacial Electrochem.* **1986**, *209*,
- 470 101–107.
- 471 [8] J. Hawecker, J.-M. Lehn, R. Ziessel, *J. Chem. Soc. {,} Chem. Commun.* **1983**, 536–538.
- 472 [9] A. Zhanaidarova, A. L. Ostericher, C. J. Miller, S. C. Jones, C. P. Kubiak,
- 473 *Organometallics* **2019**, *38*, 1204–1207.
- 474 [10] S. Cosnier, A. Deronzier, J.-C. Moutet, *J. Electroanal. Chem. Interfacial Electrochem.*
- 475 **1986**, *207*, 315–321.
- 476 [11] T. Yoshida, K. Tsutsumida, S. Teratani, K. Yasufuku, M. Kaneko, *J. Chem. Soc. {,}*
- 477 *Chem. Commun.* **1993**, 631–633.
- 478 [12] S. Oh, J. R. Gallagher, J. T. Miller, Y. Surendranath, *J. Am. Chem. Soc.* **2016**, *138*, 1820–
- 479 1823.
- 480 [13] N. M. Orchanian, L. E. Hong, J. A. Skrainka, J. A. Esterhuizen, D. A. Popov, S. C.
- 481 Marinescu, *ACS Appl. Energy Mater.* **2019**, *2*, 110–123.
- 482 [14] J. Willkomm, E. Bertin, M. Atwa, J.-B. Lin, V. Birss, W. E. Piers, *ACS Appl. Energy*
- 483 *Mater.* **2019**, *2*, 2414–2418.
- 484 [15] J. D. Blakemore, A. Gupta, J. J. Warren, B. S. Brunshwig, H. B. Gray, *J. Am. Chem.*
- 485 *Soc.* **2013**, *135*, 18288–18291.
- 486 [16] A. Zhanaidarova, S. C. Jones, E. Despagnet-Ayoub, B. R. Pimentel, C. P. Kubiak, *J. Am.*
- 487 *Chem. Soc.* **2019**, *141*, 17270–17277.
- 488 [17] K. Shen, L. Zhang, X. Chen, L. Liu, D. Zhang, Y. Han, J. Chen, J. Long, R. Luque, Y.
- 489 Li, B. Chen, *Science* **2018**, *359*, 206–210.
- 490 [18] M. Wu, Y. Li, Z. Deng, B. L. Su, *ChemSusChem* **2011**, *4*, 1481–1488.
- 491 [19] S. Suter, S. Haussener, *Energy Environ. Sci.* **2019**, *12*, 1668–1678.
- 492 [20] J.-P. Song, L. Wu, W.-D. Dong, C.-F. Li, L.-H. Chen, X. Dai, C. Li, H. Chen, W. Zou,
- 493 W.-B. Yu, Z.-Y. Hu, J. Liu, H.-E. Wang, Y. Li, B.-L. Su, *Nanoscale* **2019**, *11*, 6970–
- 494 6981.
- 495 [21] M. L. Clark, P. L. Cheung, M. Lessio, E. A. Carter, C. P. Kubiak, *ACS Catal.* **2018**, *8*,
- 496 2021–2029.
- 497 [22] B. A. Rosen, A. Salehi-Khojin, M. R. Thorson, W. Zhu, D. T. Whipple, P. J. A. Kenis,
- 498 R. I. Masel, *Science* **2011**, *334*, 643–644.
- 499 [23] D. C. Grills, Y. Matsubara, Y. Kuwahara, S. R. Golisz, D. A. Kurtz, B. A. Mello, *J. Phys.*
- 500 *Chem. Lett.* **2014**, *5*, 2033–2038.
- 501 [24] B. Qin, Y. Li, H. Fu, H. Wang, S. Chen, Z. Liu, F. Peng, *ACS Appl. Mater. Interfaces*
- 502 **2018**, *10*, 20530–20539.
- 503 [25] J. Agarwal, R. P. Johnson, G. Li, *J. Phys. Chem. A* **2011**, *115*, 2877–2881.
- 504 [26] A. J. Morris, G. J. Meyer, E. Fujita, *Acc. Chem. Res.* **2009**, *42*, 1983–1994.
- 505 [27] G. P. S. Lau, M. Schreier, D. Vasilyev, R. Scopelliti, M. Grätzel, P. J. Dyson, *J. Am.*

- 506 *Chem. Soc.* **2016**, *138*, 7820–7823.
- 507 [28] X. Zheng, G. Shen, C. Wang, Y. Li, D. Dunphy, T. Hasan, C. J. Brinker, B. L. Su, *Nat.*  
508 *Commun.* **2017**, *8*, 1–9.
- 509 [29] J. M. Smieja, C. P. Kubiak, *Inorg. Chem.* **2010**, *49*, 9283–9289.
- 510 [30] B. Reuillard, K. H. Ly, T. E. Rosser, M. F. Kuehnel, I. Zebger, E. Reisner, *J. Am. Chem.*  
511 *Soc.* **2017**, *139*, 14425–14435.
- 512
- 513